AIAA 81-0222R

Aerodynamic Jump Prediction for Supersonic, High Fineness Ratio, Cruciform Finned Bodies

Lawrence E. Lijewski*
U.S. Air Force Armament Laboratory, Eglin Air Force Base, Florida

A jump angle prediction theory is developed for supersonic free-flight missiles. Six-degree-of-freedom trajectory computations indicate that the theory accurately predicts the jump angle of finned bodies for a wide range of conditions. Initial conditions and jump angle values of actual missiles are established by range test firings of flechettes. The raw data are fitted to a fourth-order polynomial and an epicyclic motion and results put into initial condition form. The initial conditions are applied both to the theory and six-degree-of-freedom trajectory computations and results compared to target data. The agreement between the theory and test results indicate the data reduction method and theory provide an accurate means of predicting dispersion of flechettes. Initial conditions are shown to be valid at the start of free flight, generally downrange of the sabot separation. Analysis of the firing data indicates that the initial conditions result from an impulse imparted to the flechette through sabot separation and asymmetrical muzzle blast. Initial transverse linear velocity is shown to be the single most influential term in the jump equation. Maximum yaw location is shown to locate the initial conditions of free flight. Initial momentum imbalance is presented as the reason dispersion exists.

Nomenclature

Cm_α = static moment stability coefficient
$Cm_{\delta_\epsilon}\vec{\delta}_\epsilon$ = total aerodynamic asymmetry moment coefficient
$Cm_{p\beta}$ = Magnus moment stability coefficient
Cz_α = static force stability coefficient
$Cz_{\delta_\epsilon}\vec{\delta}_\epsilon$ = total aerodynamic asymmetry force coefficient
$Cz_{p\beta}$ = Magnus force stability coefficient
d = missile diameter
i = denotes z-axis component in complex system
I_x = axial moment of inertia
I_y = transverse moment of inertia
$\vec{JA}$ = complex jump angle
$\vec{K}$ = amplitude coefficient in angular motion solution
m = missile mass
M_α = static moment stability derivative
$M_{\dot\alpha}$ = lag moment stability derivative
M_{δ_ϵ} = asymmetry moment derivative
$M_{p\beta}$ = Magnus moment stability derivative
M_q = pitching velocity moment stability derivative
p = missile roll rate
$\vec{q}$ = complex angular velocity $= q + ir$
q = pitching velocity
r = yawing velocity
$\vec{S}$ = complex lateral translation $= y + iz$
t = time
u = velocity along x-axis
v = velocity along y-axis
w = velocity along z-axis
x = downrange position component
y = swerve position component
z = heave position component
Z_α = static force stability derivative
$Z_{\dot\alpha}$ = lag force stability derivative
Z_{δ_ϵ} = asymmetry force derivative
$Z_{p\beta}$ = Magnus force stability derivative
Z_q = pitching velocity force stability derivative
$\vec{\alpha}$ = complex angle of attack $= \beta + i\alpha$
α = pitch angle of attack
β = yaw angle of attack
$\vec{\delta}_\epsilon$ = aerodynamic asymmetry vector $= \delta_r + i\delta_\epsilon$
δ = angular motion phase angle
γ = axis system rotation angle
λ = angular motion damping rate
ω = angular motion frequency
ϕ = $\lambda + i\omega$
ρ = air density

Superscripts

$(\dot{})$ = derivative with respect to time
$(\,)'$ = parameter in rotated axis system

Subscripts

0 = initial condition parameter
N = nutation arm parameter
P = precession arm parameter
T = trim arm parameter
R = yaw of repose arm parameter

Presented as Paper 81-0222 at the AIAA 19th Aerospace Sciences Meeting, St. Louis, Mo., Jan. 12-15, 1981; submitted March 3, 1981; revision received Jan. 4, 1982.

*Aerodynamics Research Manager. Member AIAA.

Background

THE causes of jump and dispersion of gun-launched ballistic vehicles have been studied and investigated for many years. The definition of aerodynamic jump has been established as the deviation of a ballistic vehicle from the line of boresight at any point along a gravity-free trajectory. It follows that the jump angle is the angle between the line of boresight and a line connecting the gun tube and the ballistic vehicle along the trajectory. Early work centered around projectiles such as artillery and mortar rounds with intensive investigations into fin-stabilized saboted projectiles conducted in the relatively recent past. Derivation of the jump angle equation has gone through a number of perturbations during this time, each reflecting the state-of-the-art and the application at hand. In some of the earliest work,[1,2] the jump was attributed to the initial yaw caused by muzzle disturbance and bore clearance. Zaroodny[3] expanded the equation to include initial yawing and linear momentum terms, although he attributed the linear momentum to the gun recoil and not the blast.

The first evidence of any asymmetry term in the trajectory equation was presented by Nicolaides.[4] Further, it was found that low roll rates cause large dispersions for asymmetrical missiles.[5] Murphy later[6] expanded this work to include asymmetrical projectiles with varying roll rate, and showed the importance of transient roll behavior in jump theory.

Murphy[7] identified the jump as being generated in two distinct regions, the blast regime and the free-flight regime. The yaw and yawing terms were the only initial conditions considered while any linear momentum imparted to the projectile was ignored.[8]

With the advent of high fineness ratio, saboted, finned projectiles a new problem appeared; sabot separation effects on jump angle. Glauz[9] was one of the first to investigate the implications of sabot separation on the trajectory of a missile. He found that asymmetrical sabot separation results in an asymmetric shock pattern acting on the missile capable of imposing large angular and transverse impulses on the missile. The most recent advances[10-15] have been in the area of jump due to muzzle blast and sabot separation. Schmidt recognized the importance of the linear momentum term, and incorporated it into the jump equation.[12] However, only a component of linear momentum in the vertical axis was included, rather than a complex term.

Throughout the evolution of the jump angle equation, the initial transverse position and Magnus coefficients were deleted from the analysis. The initial transverse position has always been neglected since the origin of the axis system was thought to coincide with the initial condition position. However, with the initial conditions taken farther downstream at the commencement of free flight, the initial transverse position becomes a valid term in the jump angle equation. The Magnus coefficients have been included in previous theory derivations, but eliminated during analysis due to lack of adequate data. Remarkably, although jump angle has been studied for many years, and dispersion patterns established from generalized initial conditions, correlation of the complete theory with test data for individual rounds has not been attempted.

The Problem

Based on the review of previous efforts, it is evident that validation of the complete jump theory with initial condition and target data has not been done. The complete jump equation needs to be validated to determine the main contributing terms to jump. In addition, the point of transition between the forced response blast region and the free-flight regime has not been clearly defined with initial conditions that yield accurate target predictions. Consequently, the downrange location where free-flight begins and initial conditions occur needs to be identified. As a result, the present investigation was undertaken to address these problems.

Initially, the complete jump equation will be derived from first principles for the entire spectrum of flight conditions. The equation will then be validated with six-degree-of-freedom computer predictions. Initial flight conditions will be extracted from free-flight data for a number of locations immediately downrange of the muzzle and substituted into the jump equation to predict target impacts. From free-flight photographs and the best target predictions, the distinction between the blast and free-flight regions will be identified, and true initial conditions determined.

Figure 1 illustrates the jump angle definition adopted in this discussion. The missile analyzed is a finned body flechette with a fineness ratio of 23. Other flechette mass parameters include: $d=0.006$ ft; $m=0.000046$ slugs; $I_x=2.17\times10^{-10}$ slug-ft^2; and $I_y=3.6241\times10^{-8}$ slug-ft^2.

Theory Development

The objective of the jump angle equation derivation is to combine previous efforts into one solution and identify important parameters. Five assumptions are made initially to linearize the problem: 1) drag and gravity are neglected for the flight ranges and supersonic velocities discussed here; 2) roll rate is constant; 3) all force and moment coefficients dependent on angle of attack are linear with angle of attack;

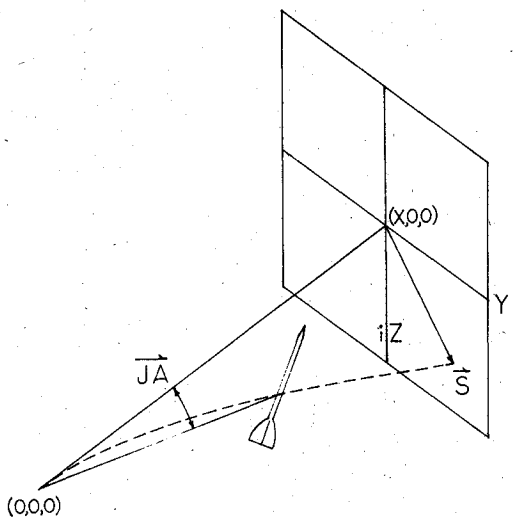

Fig. 1 Jump angle-trajectory relationship.

4) all force and moment coefficients independent of angle of attack are constant; and 5) products of force and moment coefficients are negligible, except those involving Z_{δ_ϵ} and M_{δ_ϵ}.

Given the complex differential equations of motion for a nonaccelerating missile ($\dot{u}=0$, $\dot{p}=0$) written in terms of the aeroballistic axes,

$$Z_\alpha\vec{\alpha}+iZ_q\vec{q}+Z_{\dot{\alpha}}\vec{\dot{\alpha}}+ipZ_{p\beta}\vec{\alpha}+Z_{\delta_\epsilon}\vec{\delta}_\epsilon e^{ipt}=mu(\vec{\dot{\alpha}}-i\vec{q}) \tag{1a}$$

$$-iM_\alpha\vec{\alpha}+M_q\vec{q}-iM_{\dot{\alpha}}\vec{\dot{\alpha}}+pM_{p\beta}\vec{\alpha}-iM_{\delta_\epsilon}\vec{\delta}_\epsilon e^{ipt}=I_y\vec{\dot{q}}-ipI_x\vec{q} \tag{1b}$$

the solution of quadricyclic angular motion,

$$\vec{\alpha}=\vec{K}_N e^{\phi_N t}+\vec{K}_p e^{\phi_P t}+\vec{K}_T e^{ipt}+\vec{K}_R \tag{2}$$

and the trajectory equation for free-flight motion,

$$\vec{\dot{S}}=u(\vec{\dot{\alpha}}-i\vec{q}) \tag{3}$$

the solution is obtained by neglecting small terms and applying the assumptions.

$$\vec{S}=\vec{S}_0+\left[\vec{\dot{S}}_0-\left(\frac{Z_\alpha+ipZ_{p\beta}}{mu}\right)\left(\frac{\vec{K}_N}{\phi_N}+\frac{\vec{K}_P}{\phi_P}\right)\right]t$$
$$+\left[\left(\frac{Z_\alpha+ipZ_{p\beta}}{mu}\right)\vec{K}_T+\frac{Z_{\delta_\epsilon}\vec{\delta}_\epsilon}{m}\right]\int_0^t\int_0^t(e^{ipt}\mathrm{d}t)\,\mathrm{d}t \tag{4}$$

High Roll Rate Approximation

The double integral in Eq. (4) integrates to

$$\int_0^t\int_0^t(e^{ipt}\mathrm{d}t)\,\mathrm{d}t=\frac{e^{ipt}}{(ip)^2}-\frac{t}{ip}-\frac{1}{(ip)^2} \tag{5}$$

When the roll rate is large, the first and third terms are small compared to the second term, reducing Eq. (4) to

$$\vec{S}=\vec{S}_0+\left[\vec{\dot{S}}_0-\left(\frac{Z_\alpha+ipZ_{p\beta}}{mu}\right)\left(\frac{\vec{K}_N}{\phi_N}+\frac{\vec{K}_P}{\phi_P}+\frac{\vec{K}_T}{ip}\right)+\frac{iZ_{\delta_\epsilon}\vec{\delta}_\epsilon}{mp}\right]t \tag{6}$$

By substituting known aerodynamic relationships for K_N, K_P, K_T, ϕ_N, ϕ_P, and applying the definition of the mil-angle, which is the angle subtended by a 1 ft dispersion at 1000 ft of range, Eq. (6) becomes

$$\vec{JA} = \frac{1000}{x}\left\{\vec{S}_0 + \vec{S}_0\left(\frac{x}{u}\right) + iCz_{\delta_\epsilon}\vec{\delta}_\epsilon\left(\frac{\rho u\pi d^2 x}{8mp}\right) - Ax\frac{I_y}{mud}\left[\vec{\alpha}_0 - \vec{\alpha}_0\left(\frac{ipI_x}{I_y}\right) - Cm_{\delta_\epsilon}\vec{\delta}_\epsilon\left(\frac{\rho u^2\pi d^3}{8pI_y}\right) - Cz_{\delta_\epsilon}\vec{\delta}_\epsilon\left(1-\frac{I_x}{I_y}\right)\left(\frac{\rho u\pi d^2}{8m}\right)\right]\right\} \quad (7)$$

where

$$A = \frac{Cz_\alpha + iCz_{p\beta}\dfrac{pd}{2u}}{Cm_\alpha + Cz_{p\beta}\dfrac{pd}{2u}\dfrac{pI_x}{mud} + i\left[Cm_{p\beta}\dfrac{pd}{2u} - Cz_\alpha\dfrac{pI_x}{mud}\right]} \quad (8)$$

Equation (7) approximates the jump angle for high roll rate applications with slight configurational asymmetries at any x-location downrange.

Low Roll Rate Approximation

For roll rates generally less than $0.02u_0$ but greater than zero, Eq. (4) can be reduced to another approximation. All three terms in Eq. (5) are significant resulting in an Eq. (7) with $\cos(px/u) + i\sin(px/u)$ substituted for e^{ipt},

$$\vec{JA} = \frac{1000}{x}\left\{\vec{S}_0 + \vec{S}_0\left(\frac{x}{u}\right) - \frac{xI_y}{mud}\left(\frac{Cz_\alpha}{Cm_\alpha}\right)\vec{\alpha}_0 + \frac{\rho u^2\pi d^2}{8m}\left[Cz_{\delta_\epsilon}\vec{\delta}_\epsilon - i\left(\frac{Cz_\alpha}{Cm_\alpha}\right)Cm_{\delta_\epsilon}\vec{\delta}_\epsilon\right]\left[\frac{1}{p^2}\left(1-\cos\left(\frac{px}{u}\right)\right) + \frac{i}{p}\left(\frac{x}{u} - \frac{\sin(px/u)}{p}\right)\right]\right\} \quad (9)$$

The initial condition $\vec{\alpha}_0$, a small contributor to jump even at high roll rate, has been dropped since it is multiplied by the low roll rate.

Near Zero Roll Rate Approximation

For the case of zero roll, Eq. (9) is inadequate due to p in the denominator. To overcome this problem, $\sin(px/u)$ and $\cos(px/u)$, are approximated by the first four terms of the power series, yielding,

$$\vec{JA} = \frac{1000}{x}\left\{\vec{S}_0 + \vec{S}_0\left(\frac{x}{u}\right) - \frac{xI_y}{mud}\left(\frac{Cz_\alpha}{Cm_\alpha}\right)\vec{\alpha}_0 + \frac{\rho\pi d^2x^2}{16m}\left[Cz_{\delta_\epsilon}\vec{\delta}_\epsilon - i\left(\frac{Cz_\alpha}{Cm_\alpha}\right)Cm_{\delta_\epsilon}\vec{\delta}_\epsilon\right] \times\left[\left(1-\frac{1}{12}\left(\frac{px}{u}\right)^2 + \frac{1}{360}\left(\frac{px}{u}\right)^4\right) + i\left(\left(\frac{px}{3u}\right) - \frac{1}{60}\left(\frac{px}{u}\right)^3 + \frac{1}{2520}\left(\frac{px}{u}\right)^5\right)\right]\right\} \quad (10)$$

Equation (10) is effective from zero roll rate up to roll rates where $(px/u) = 2$. Values of (px/u) greater than 1 tend to be less accurate than the low roll rate approximation, Eq. (9).

Theory Validation

Initial Conditions

The theoretical approximations of jump angle, Eqs. (7), (9), and (10), indicate that jump depends upon initial conditions, aerodynamic coefficients, and mass parameters. To assure that the three equations are valid, and to determine the importance of the individual terms, theoretical results were compared to six-degree-of-freedom (6-DOF) computer program results. A total of 189 cases were run by varying the initial conditions, $\vec{S}_0$, $\vec{\alpha}_0$, $\dot{\vec{\alpha}}_0$, p_0, u_0, as well as Magnus and asymmetry coefficients. Table 1 lists 12 typical cases. The initial conditions were varied to reflect the minimum and maximum limits the flechette might see in flight, while the asymmetry coefficients were set to zero for these cases. The target was chosen to be at 1000 ft downrange for convenience. The governing equation for these cases is a reduced Eq. (7):

$$\vec{JA} = \frac{1000}{x}\left[\vec{S}_0 + \vec{S}_0\left(\frac{x}{u}\right) - \frac{xI_y}{mud}A\left(\dot{\vec{\alpha}}_0 - \frac{ipI_x}{I_y}\vec{\alpha}_0\right)\right] \quad (11)$$

The comparisons show good to excellent agreement. Case 1 verifies that zero initial conditions yield zero jump. Cases 2-4 show that initial transverse velocity can affect jump significantly. Although the value used for validating the theory may be high based on actual test results, a value of 15 ft/s would still yield a three mil jump angle. Cases 5-7 indicate small dispersion from a moderate angle of attack. The disagreement between the theory and 6-DOF computer calculations is most notable here because of the small values involved. Cases 8-10 indicate a significant effect on jump by initial angular rate. Although 250 rad/s is slightly higher than test results show, a jump angle of 1.5 mils due to initial angular rate would not be uncommon. All three initial conditions with Magnus coefficient are presented in cases 11 and 12. The effect of Magnus on jump is not apparent in these cases, and needs to be examined more closely.

Magnus Coefficients

The Magnus force and moment coefficients enter into the jump equation through Eq. (8). By inspecting the individual terms, for the case of the flechette, the terms that include (pI_x/mud) are an order of magnitude smaller than neighboring terms. In addition, data from similar shaped missiles[16] indicate that $Cz_{p\beta}$ is small compared to Cz_α even though $Cm_{p\beta}$ is similar in magnitude to Cm_α. With these assumptions, Eq. (8) becomes:

$$A = \frac{Cz_\alpha}{Cm_\alpha + i(pd/2u)Cm_{p\beta}} \quad (12)$$

To evaluate the Magnus effect, Eq. (12) is substituted into Eq. (11) and $\vec{S}_0$, $\dot{\vec{S}}_0$, and $\vec{\alpha}_0$ are set to zero. Although $\vec{\alpha}$ is also multiplied by the factor A, the important contribution to jump is by $\dot{\vec{\alpha}}_0$, as shown by the validations in Table 1. For a given configuration, the change in the complex jump angle for various ratios of $Cm_{p\beta}/Cm_\alpha$ and a range of initial angular rates is shown in Fig. 2. The $pd/2u$ parameter was set at 0.09 to reflect an initial velocity of 1000 ft/s, the steady-state flechette roll rate, and flechette mass parameters. As the curves in Fig. 2 show, the Magnus effect can be profound, matching the magnitude of the observed jump in test firings. However, since this evaluation is flechette dependent, other configurations must be considered individually to determine the effect of Magnus. In these individual evaluations, all the terms in Eq. (8) should be considered.

Aerodynamic Asymmetry

The asymmetry terms in Eqs. (7), (9), and (10) were validated by varying the roll rate from the steady-state flechette roll rate down to zero for various initial conditions.

Table 1 Theory validation of initial conditions and symmetric missile aerodynamic coefficients

CASE	INITIAL CONDITIONS					COEFFICIENTS		$\vec{JA}$ (mils)	
	$\vec{\dot{S}}_o$	$\vec{\alpha}_o$	$\vec{\dot{\alpha}}_o$	p_o	u_o	Cz_α Cm_α $Cm_q + Cm_{\dot{\alpha}}$	$Cz_{p\beta}$ $Cm_{p\beta}$	6-DOF	THEORY
1	0	0	0	all	all	✓	✓	0 + 0i	0 + 0i
2	100+ 100i	0	0	all	5000	✓	0	20.002+ 20.006i	20.000+ 20.000i
3	100+ 100i	0	0	all	3000	✓	0	33.346+ 33.368i	33.333+ 33.333i
4	100+ 100i	0	0	all	1000	✓	0	100.254+ 100.765i	100.000+ 100.000i
5	0	5+ 5i	0	31416	5000	✓	0	-0.566+ 0.031i	-0.136+ 0.136i
6	0	5+ 5i	0	18850	3000	✓	0	-0.448+ 0.036i	-0.075+ 0.079i
7	0	5+ 5i	0	6283	1000	✓	0	-0.123+ 0.354i	-0.072+ 0.079i
8	0	0	250+ 250i	31416	5000	✓	0	-2.027 -2.034i	-2.073 -2.073i
9	0	0	250+ 250i	18850	3000	✓	0	-1.962 -1.966i	-1.970 -1.970i
10	0	0	250+ 250i	6283	1000	✓	0	-5.254 -5.250i	-5.540 -5.540i
11	100+ 100i	5+ 5i	250+ 250i	31416	5000	✓	✓	17.738+ 17.504i	17.783+ 18.050i
12	100+ 100i	5+ 5i	250+ 250i	18850	3000	✓	✓	30.428+ 30.818i	31.206+ 31.458i

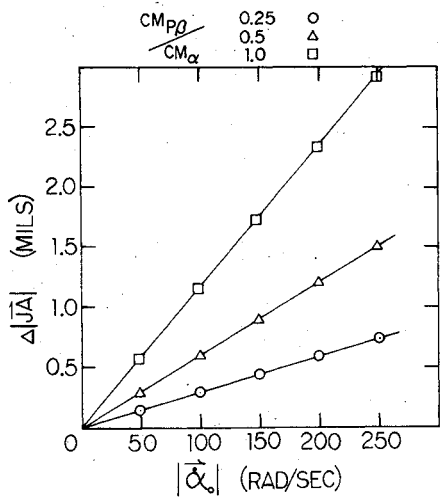

Fig. 2 Magnus effect on jump angle.

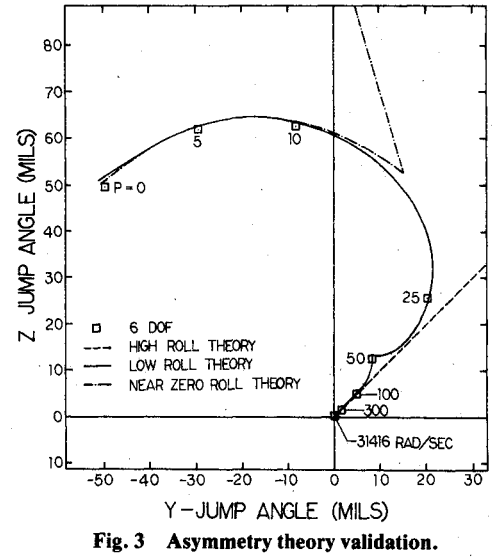

Fig. 3 Asymmetry theory validation.

The asymmetry coefficients were selected to reflect a 1 deg nonrolling trim to exist in free flight. Figure 3 illustrates the agreement between the theory and the 6-DOF computer calculations for a typical case. All initial conditions were set to zero to show the effect of the aerodynamic asymmetry alone, with the launch velocity at 5000 ft/s. The agreement is excellent for all three theories in their respective ranges; high roll theory down to $0.02u_0$, low roll down to nearly zero roll, and the zero roll theory from $pt=2$ down to zero roll. Although Fig. 3 depicts only a few data points, a large number of other cases were run with similar results that back up the theory validity and roll rate ranges. The launch velocity and initial conditions were varied for those cases.

Test Firings and Data Reduction

To correlate the validated theory with test data, a series of free-flight trajectory firings[17] were conducted to obtain target impact and initial condition data. The test setup allowed both translational and angular data to be taken as a function of time. The gun barrel was mounted on a steel girder to eliminate "barrel whip" due to recoil, and was boresighted on a target 50 ft downrange. Orthogonal x-ray photographs were taken at 1, 3, 5, 7, 9, and 11 ft downrange to provide swerve, heave, pitch, and yaw data.

From the battery of test firings, eight representative rounds were selected for analysis. The translational data were fitted to a fourth-order polynomial by a least-squares method. Probable errors of less than 1% were observed. The y-direction data were fit separately from the z-direction data to distinguish between the heave and swerve components. The resulting equations of the fitted curves were then differentiated to obtain the equations for the transverse velocities v and w in the y and z directions. From the y and z results, the transverse conditions, $\vec{S}$ and $\dot{\vec{S}}$, could then be expressed in complex form for any location up to 11 ft downrange.

To obtain the angular conditions, $\vec{\alpha}$ and $\dot{\vec{\alpha}}$, the polynomial fit technique was unacceptable due to large errors in fitting. The most desirable method would be to fit the raw data to the well-known three-degree-of-freedom, tricyclic motion equation[4,16] by a least-squares fit. However, the availability of only six data points, and generally less than one period of oscillatory motion eliminated this method from consideration. By examination of the plots of raw angular data, it was noted that the motions tend to be planar or one-degree-of-freedom motions in nature for the first 11 ft downrange. By rotating the axis system to coincide with the dominant angular mode, Fig. 4, the motion was fit to a one-degree-of-freedom epicyclic motion,[18,19] Eq. 13.

$$\alpha' = K' e^{\lambda t} \cos(\omega t + \delta) \tag{13}$$

Simple differentiation of Eq. (13) yields an expression for $\dot{\alpha}'$. By resolving α' and $\dot{\alpha}'$ back into the α, β axis system, values for $\alpha, \beta, \dot{\alpha}, \dot{\beta}$ can be resolved and combined to form the complex terms $\vec{\alpha}$, $\dot{\vec{\alpha}}$. The probable error of fit is less than 5% for α', but no doubt larger for $\dot{\alpha}'$ since it is a result of differentiating a fitted equation.

Flight Data Analysis

To compare the theory with the test data, the initial conditions for each round had to be determined. Pin-pointing the initial conditions, however, is a difficult task since they occur somewhere downrange of the muzzle at the beginning of free flight. To locate the region of free-flight commencement, a series of jump angle calculations from Eq. (11) were made with initial conditions generated from the $\vec{S}$, $\dot{\vec{S}}$, $\vec{\alpha}$, and $\dot{\vec{\alpha}}$ equations obtained through the data reduction methods. These initial conditions were determined for each round at locations 1 through 11 ft downrange. Results are presented in Fig. 5. The test data symbols represent actual target impacts while the theory and 6-DOF symbols correspond to target impact predictions. The numbers next to the symbols indicate the location downrange where the initial conditions were chosen to make the impact predictions. The excellent agreement between theory and 6-DOF results indicate that the assumptions made and terms neglected throughout the theory development were proper. The theory and flight data comparisons, in general, show good agreement for a downrange location between 1 and 11 ft from the gun muzzle. The location of best agreement between theory and data lies between 2 and 5 ft downrange for all rounds except 7 and 8. This is the first indication where free flight begins: between 2 and 5 ft downrange. The typical flight transition sequence, Fig. 6, supports this observation by indicating that sabot separation occurs between 1 and 5 ft downrange of the muzzle. The flight transition sequence for every round shows that the sabot has separated and nearly cleared the flechette at 3 ft. Flechette-sabot mechanical interference is a possibility at 3 ft but aerodynamic interference is a near certainty. Investigations by Glauz[9] and Schmidt[14,15] conclude that aerodynamic interference is an important factor in jump angle determination.

By 5 ft downrange, the sabot has separated and completely cleared the flechette with the flechette appearing to be in free flight. Assuming that free flight begins between sabot separation and 5 ft downrange, fair to excellent agreement is seen in Fig. 6 for rounds 4, 6, 14, 16, 17, and 19. Rounds 4 and 19 show only fair agreement (1-2 mils difference) with target data. These two rounds exhibited large angular motions that amplified the error in $\dot{\vec{\alpha}}_0$, resulting in loss of accuracy in the target predictions. The fact that the target prediction patterns match the direction of the angular motion supports

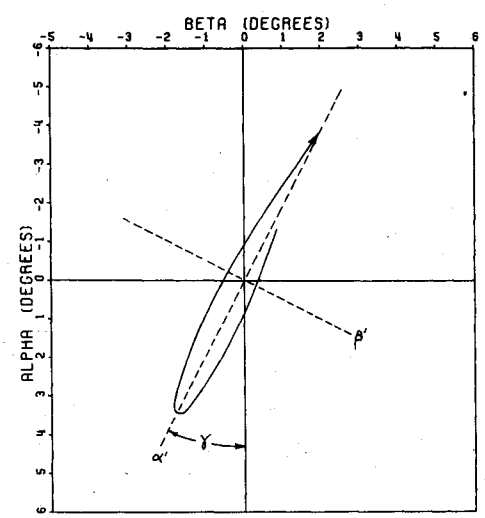

Fig. 4 Pure pitching motion approximation.

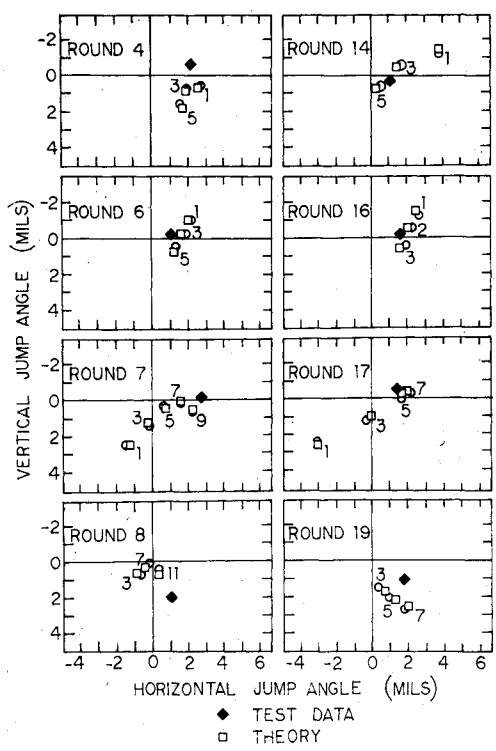

Fig. 5 Jump angle target predictions and data.

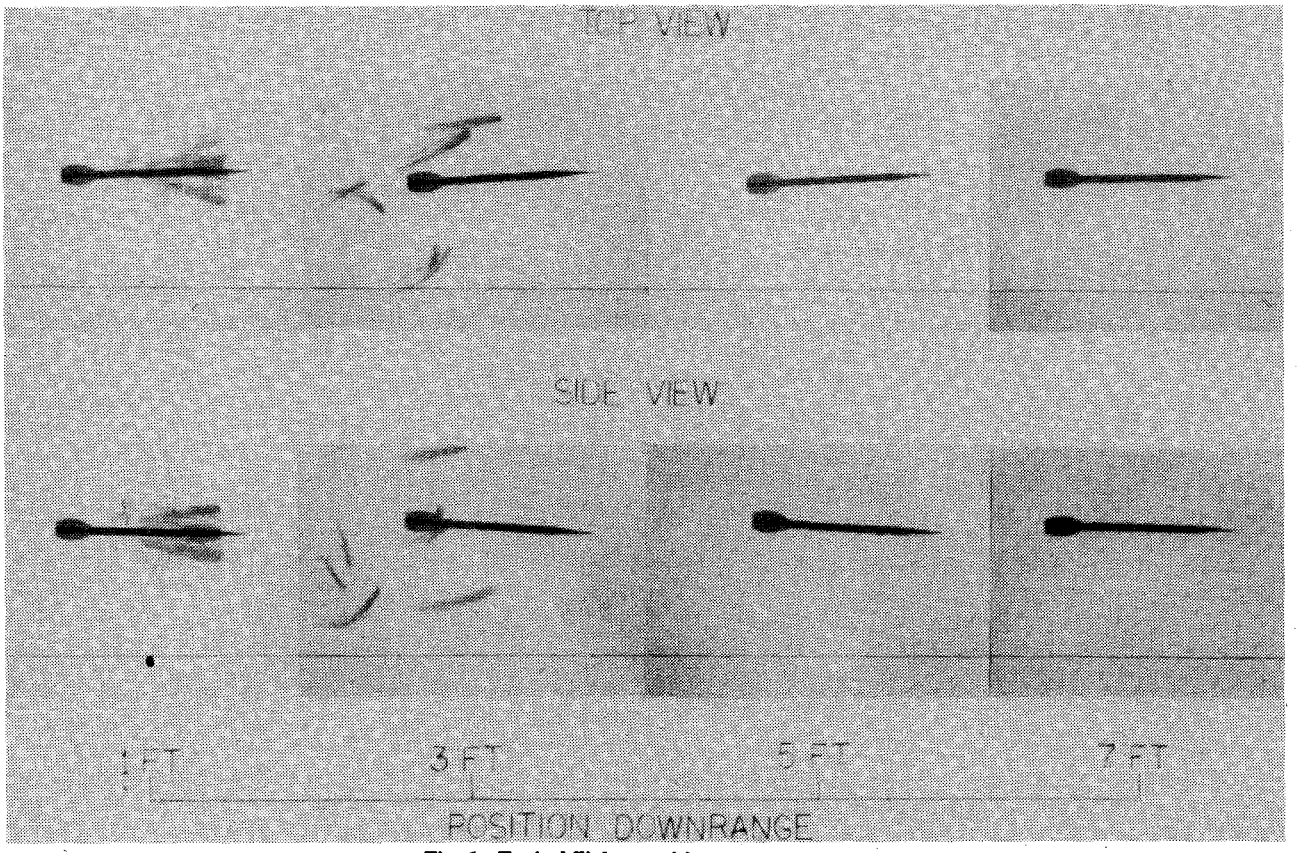

Fig. 6 Typical flight transition sequence.

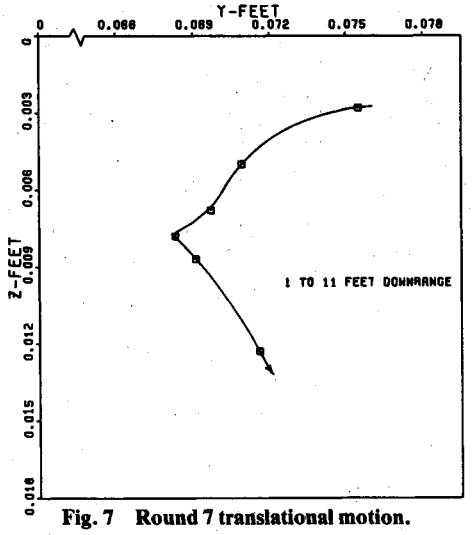

Fig. 7 Round 7 translational motion.

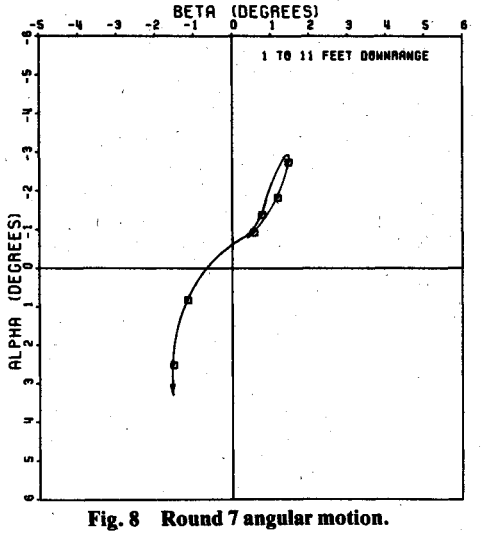

Fig. 8 Round 7 angular motion.

this contention. This coupling between prediction patterns and angular motion exists for all rounds, with a smaller range of $\vec{\alpha}_0$ for the other rounds resulting in smaller errors and better predictions.

Sabot separation is only one factor that can affect the initialization of free flight. Schmidt[10] showed that asymmetrical muzzle jets can significantly affect the missile in the blast region and, therefore, the resulting jump. Figure 6 does present some evidence of an asymmetrical blast by the sabot petal pattern at 3 ft downrange. In addition, round 7 presents an interesting case. Both the translational and angular data, Figs. 7 and 8, indicate a discontinuity in the motions at about 7 ft downrange. Since the sabot has separated and cleared the flechette by 5 ft downrange, it is conjectured that an asymmetrical blast has caused this discontinuity. The nature and structure of this asymmetrical flow is unknown, but Figs. 7 and 8 give strong evidence as to its existence. The plot of round 7 in Fig. 5 supports this observation with the best jump angle prediction occurring between 7 and 9 ft downrange.

Round 8 shows best agreement in Fig. 5 when initial conditions are taken at 11 ft downrange. Since data are not available farther downrange, it is unknown whether better agreement could be obtained past 11 ft downrange. The possibility of an asymmetrical muzzle blast affecting the flechette past 11 ft downrange would certainly account for the poor agreement seen in round 8, but the data up to 11 ft does not give obvious evidence of an asymmetrical muzzle blast.

Initial Condition Contributions

The relationships of the initial conditions to the observed jump are worth mentioning. Previous work[20] has proposed that a linear relationship exists between the first maximum

yaw and the observed jump. Figure 9 presents a plot of first maximum yaw vs jump angle for the eight rounds tested. Clearly from these data no linear relationship exists. However, inspection of the angular motions of each round indicate that the location of the best theory/data agreement in Fig. 5 coincide with a maximum yaw of the round, Fig. 10. The brackets around each symbol indicate the span of downrange locations where the maximum yaw or best prediction initial conditions occur. The magnitude of the first maximum yaw does not predict the jump angle magnitude, but the location of the first maximum yaw in free flight tends to yield the best initial conditions, which yield the best target predictions. Therefore, the location of the first maximum yaw tends to coincide with the initiation of free flight.

The relative influence that each initial condition has on the jump angle was determined by averaging the individual jump angle contributions of all eight rounds when the initial conditions are chosen that give the best predictions. The transverse linear and angular velocities were found to be the most important, comprising 64% and 27% of the jump angles. The initial angle of attack and transverse position are found to contribute only 5% and 4% to the jump angle respectively. Previous work[5] assigned initial transverse velocity to blast jump and initial angular velocity to aerodynamic jump. Equation (11) combines these two initial conditions in one equation for jump. These initial conditions, as well as initial angle of attack and transverse position, are generated in the blast region, but are manifested in the initial free-flight aerodynamic region. Evidence of a quantity describing blast jump is the initial transverse position, $\vec{S}_0$. This term represents the deviation of the missile center of gravity from the gun-target line to its x,y,z location upon entering free flight. The contribution of initial transverse position to jump indicates that jump attributed to the blast is small. This is confirmed by previous work of Fansler and Schmidt.[11,12,15] An interesting fact can be extracted from Eq. (11) by setting the jump angle to zero and rearranging terms.

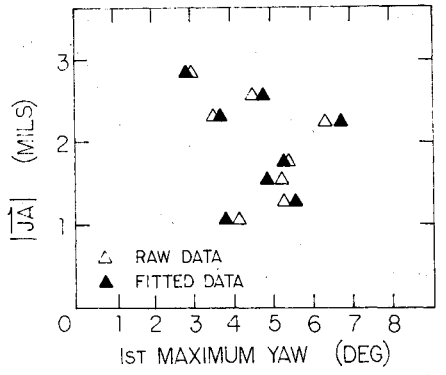

Fig. 9 Jump angle target predictions vs first maximum yaw.

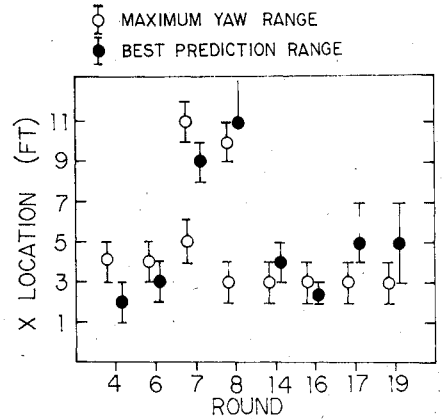

Fig. 10 Downrange locations of maximum yaw and best target prediction initial conditions.

$$m[\vec{S}_0(u/x)+\vec{S}_0]=(A/d)\,[\vec{\alpha}_0 I_y-\vec{\alpha}_0 ipI_x] \qquad (14)$$

A dimensional analysis of Eq. (14) reveals units of momentum for each term involving an initial condition. With the transverse initial conditions on the left side of the equation, and angular initial condition terms on the right, the zero jump angle condition can be summarized: the initial linear momentum equals the initial angular momentum. The observation that the initial linear and angular momentum tend to cancel each other was noted by Gallagher,[21] but he excluded sabot separation. It was thought that sabot separation was not part of the initial momentum. Equation (14) includes all physical contributions to jump for a symmetric missile since the initial conditions are defined to exist at the commencement of free flight, and out of influence from external forces.

Obviously, an infinite number of conditions satisfy Eq. (14), but it is interesting that even large values of the initial conditions can result in zero jump. Of course the smaller the terms, the better chance of satisfying the equation. Essentially, an initial momentum imbalance yields a nonzero jump angle.

Conclusions

The jump angle equation was re-derived to include initial conditions $\vec{S}_0$, $\dot{\vec{S}}_0$, $\vec{\alpha}_0$, $\dot{\vec{\alpha}}_0$, as well as Magnus and configurational asymmetry coefficients. Three distinct jump angle equations were developed to handle configurational asymmetries at all roll rates. The equations were validated by comparing results of the theories with a six-degree-of-freedom trajectory computer program for 189 cases. The contribution of Magnus was shown to be significant for given combinations $(pd/2u)$, magnitude of the Magnus force and moment coefficients, and initial angular rates. Magnus coefficients should be included in jump angle calculations unless determined to be negligible. The contribution of configurational asymmetries to jump, caused by a trim angle of 1 deg, were shown to have little effect on the high rolling flechettes, but would have significant effects for slower rolling missiles.

For the first time, all four initial conditions of free-flight flechette data were successfully used to predict target impact points of individual rounds. The favorable agreement between theory predictions and target data lend credence to the method of extracting initial conditions from the translational and angular motion of the missile the first few feet downrange of the muzzle. Results indicate that free flight generally begins immediately after sabot separation. However, some evidence was presented that an asymmetrical muzzle blast may have the ability to affect the flechette up to 9 ft downrange.

The location of the first maximum yaw downrange of the sabot separation was shown to coincide generally with the commencement of free flight. Initial conditions chosen at that location give the best target impact predictions. However, the magnitude of the first maximum yaw was shown to have no relation to the jump angle magnitude.

The initial transverse linear velocity and angular rate were shown to be the most influential conditions with the transverse velocity contributing an average 64% of the total jump, and the angular rate contributing 27%. The transverse position and angle of attack terms comprise 4% and 5% of the total jump.

Finally, the criterion for zero jump was shown to be the equality of initial linear and angular momentum. This assumes that all external forces have concluded acting on the symmetric missile. Regardless of the magnitude of the initial conditions, initial momentum balance results in zero jump. Hence, jump is the result of initial momentum imbalance.

References

[1] Fowler, R.M., Gallop, E.G., Lock, C.N.M., and Richmond, N.W., "Aerodynamics of a Spinning Shell," *Proceedings of the Royal Society of London*, Series A, Vol. 221, 1920, pp. 295-387.

[2]Sterne, T.E., "On Jump Due to Bore Clearance," BRL Report No. 491, Sept. 1944.

[3]Zaroodny, S.J., "On Jump Due to Muzzle Disturbances," BRL Report No. 703, June 1949.

[4]Nicolaides, J.D., "On the Free-Flight Motion of Missiles Having Slight Configurational Asymmetries," BRL Report No. 858, June 1953.

[5]Hunter, M.W., Shef, A., and Black, D.V., "Some Recent Aerodynamics Techniques in Design of Fin-Stabilized Free-Flight Missiles for Minimum Dispersion," *Journal of Aeronautical Sciences,* June 1956, pp. 571-577.

[6]Murphy, C.H., "Comments on Projectile Jump," BRL Memo Report No. 1071, April 1957.

[7]Murphy, C.H. and Bradley, J.W., "Jump Due to Aerodynamic Asymmetry of a Missile with Varying Roll Rate," BRL Report No. 1077, May 1959.

[8]Murphy, C.H., "Free-Flight Motion of Symmetric Missiles," BRL Report No. 1216, July 1963.

[9]Glauz, W.D., "Estimation of Forces on a Flechette Resulting from a Shock Wave," Midwest Research Institute, Kansas City, Mo., Final Report on Frankford Arsenal Contract No. DAAA25-70-C0655, May 1971.

[10]Schmidt, E.M., "The Effect of Muzzle Jet Asymmetry on Projectile Motion," BRL Report No. 1756, Jan. 1975.

[11]Fansler, K.S. and Schmidt, E.M., "The Influence of Muzzle Gasdynamics Upon the Trajectory of Fin-Stabilized Projectiles," BRL Report No. 1793, June 1975.

[12]Fansler, K.S. and Schmidt, E.M., "Muzzle Blast Influence on Trajectory of Asymmetrical Fin-Stabilized Projectiles," BRL Memo Report No. 2646, Aug. 1976.

[13]Schmidt, E.M., Fansler, K.S., and Shear, D.D., "Trajectory Perturbations of Fin-Stabilized Projectiles Due to Muzzle Blast," *Journal of Spacecraft and Rockets,* Vol. 14, June 1977, pp. 339-344.

[14]Schmidt, E.M. and Shear, D.D., "Aerodynamic Interference During Sabot Discard," BRL Report, No. 2019, Sept. 1977.

[15]Schmidt, E.M., "Measurement of Sabot Discard and Analysis of Associated Launch Disturbances," BRL Technical Report TR-02157, April 1979.

[16]Nicolaides, J.D., "Free-Flight Dynamics," Text, Aerospace Engineering Dept., Univ. of Notre Dame, 1964.

[17]Nicolaides, J.D., Ingram, C.W., Lijewski, L.E., Garsik, M.J., "On the Accuracy of Flechettes by Dynamic Wind Tunnel Tests, by Theory and Analysis, and by Actual Firings," Frankford Arsenal-TT-75005, Jan. 1975.

[18]Ingram, C.W. and Eikenberry, R.S., "A Computer Program to Fit the Initial Angular Data from Test Firing of Flechettes," Univ. of Notre Dame unpublished report, 1973.

[19]Eikenberry, R.S., "Analysis of the Angular Motion of Missiles," Univ. of Notre Dame, Sandia Laboratories SC-CR-70-6051, Feb. 1970.

[20]Piddington, M., "The Aerodynamic Characteristics of a SPIW Projectile," BRL Memo Report No. 1594, Sept. 1964.

[21]Gallagher, W.J., "Elements Which Have Contributed to Dispersion in the 90/40 mm Projectile," BRL Report No. 1013, March 1957.